Astronomical masers

OH first molecular maser Weaver et al 1963, 65.
hydroxyl Strong, varying, narrow line radio signals.
"Mysterium". Aliens?

Other common 'masing molecules':
H_2O, SiO.

Others

CH	HCN	CH_3OH	H_2CO	NH_3
methine	hyd. cyanide	methanol	formaldehyde	ammonia

Masing condition is

$$\frac{n_u}{n_L} > \frac{g_u}{g_L}$$

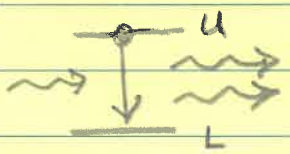

This means $T_{ex} < 0$ in Boltz factor $e^{-E_{uL}/kT_{ex}}$.
↑ what is this?

Maser characteristics

1. High T_b in maser line
   brightness temp ← what is this?
   eg OH $T_b \sim 10^{10}$ K, $H_2O \sim T_b \sim 10^{14}$ K
2. Small "hot spot" regions
   $\lesssim$ 10 AU need VLBI
3. Variable weeks/months
4. Narrow lines $\Delta v \sim 0.1$ km/s
   $\Rightarrow T_{Doppler} \lesssim 10$ K.
5. Highly polarized, up to 100% circ in OH

Megamasers Jeremy Darling expert

Found in starburst nuclei in merging galaxies, which are also ULIRGs Ultra-Luminous IR Galaxies.
First OH megamaser 1982 Arp 220 (IC 4553)
luminosity $\sim 10^3 L_\odot$

$\gtrsim 100$ known OH megamasers $T_b \sim 10^6 - 10^7$ K

Other known megamaser molecules:
H_2O CH H_2CO

H_2O

Masing lines are rotational transitions in ground elec/vib state

Most prominent line is

o-H_2O $6_{16} - 5_{23}$ 22.2 GHz = 1.35 cm^{-1}

↑ rot. levels happen to be especially close

ortho = spin triplet

Classic example:

NGC 4258 (M106)

Miyoshi + (1995) Nature 373, 127.

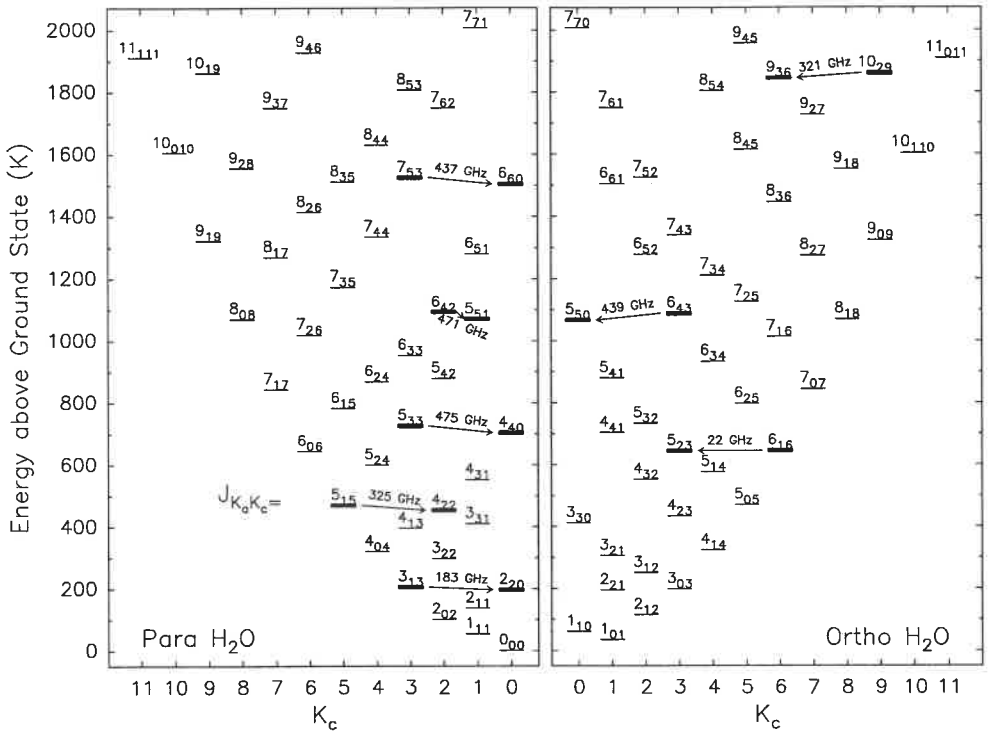

Fig. 2. Energy level diagram of para H_2O (left) and ortho H_2O (right). Upper and lower levels of known maser lines appear in bold, are connected by arrows and have the rounded transition frequency (in GHz) indicated. Data for all these lines (except for the 183 GHz line) are reported in the present paper.

the employed double sideband receivers (see Fig. 1). The radiation was analyzed with the MPIfR Fast Fourier Transform spectrometer, which provides 16384 frequency channels over the 1 GHz intermediate frequency bandwidth (Klein et al. 2006). To increase the signal to noise ratio, the spectra were smoothed to effective velocity resolutions appropriate for the measured linewidths, typically $\sim$ 0.5–1 km s^{-1}. To check the telescope pointing, the receiver was tuned to the 437 GHz H_2O line, which showed strong emission in all of our three sources, and five point crosses centered on the stellar position with half beamwidth offsets in elevation and azimuth were measured. Pointing corrections were derived from the latter measurements. The pointing was found to be accurate to within $\approx 3''$, acceptable given the FWHM beam size, θ_B, which is 20″ FWHM at 321 GHz and 13″ at 475 GHz.

Additional data had been taken earlier toward VY CMa for the 355 GHz line (see Table 1) for which maser action had been predicted by excitation modeling (see 4.4). These observations were made in 2005 July/August.

In Table 2 we present our line intensities in a flux density scale (i.e., in Janskies) assuming the aperture efficiencies observationally determined by Güsten et al. (2006) for the respective frequency ranges.

Observations of the 22.2 GHz $6_{16} - 5_{23}$ transition were made with the Effelsberg 100m telescope on 2006 June 27, i.e., ca. 1–2 weeks after the submillimeter observations. The line was detected with the facility high electron mobility transistor receiver and autocorrelator backend. The data were corrected for atmospheric opacity and variations of the telescope's gain curve with elevation.

Fig. 2 shows our observed H_2O lines on energy level diagrams of para and ortho water.

Table 1. Ground-state water maser lines observed with APEX.

H_2O $J'_{K'_aK'_c} - J''_{K''_aK''_c}$ =	Frequency (MHz)	E_ℓ/k (K)
$6_{16} - 5_{23}$	22235.08	642.5
$10_{29} - 9_{36}$	321225.64	1845.9
$5_{15} - 4_{22}$	325152.92	454.4
$17_{4,13} - 16_{7,10}$	354808.9	5764.3
$7_{53} - 6_{60}$	437346.67	1503.7
$6_{43} - 5_{50}$	439150.81	1067.7
$7_{52} - 6_{61}$	443018.30	1503.7
$6_{42} - 5_{51}$	470888.95	1041.8
$5_{33} - 4_{40}$	474689.13	702.3

Columns are (from left to right) quantum numbers of upper and lower state, frequency and energy above ground of lower state in Kelvins; k is the Boltzmann constant. Frequency values, taken from the JPL catalog, have formal uncertainties of order 50 kHz. More accurate values from a fit to the H_2O spectrum have been presented by Chen et al. (2000). The difference between their values and the ones used by us is typically of order 20 kHz, corresponding to less than 0.02 km s^{-1}, which is smaller than the uncertainties in our velocity determinations.

OH

Masing lines are in ground elec/vib/rot level.

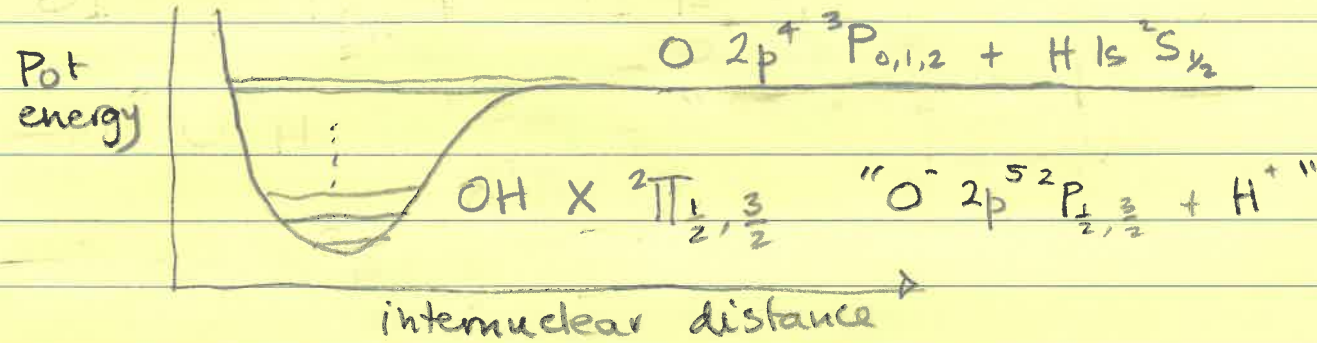

Hund case (a)

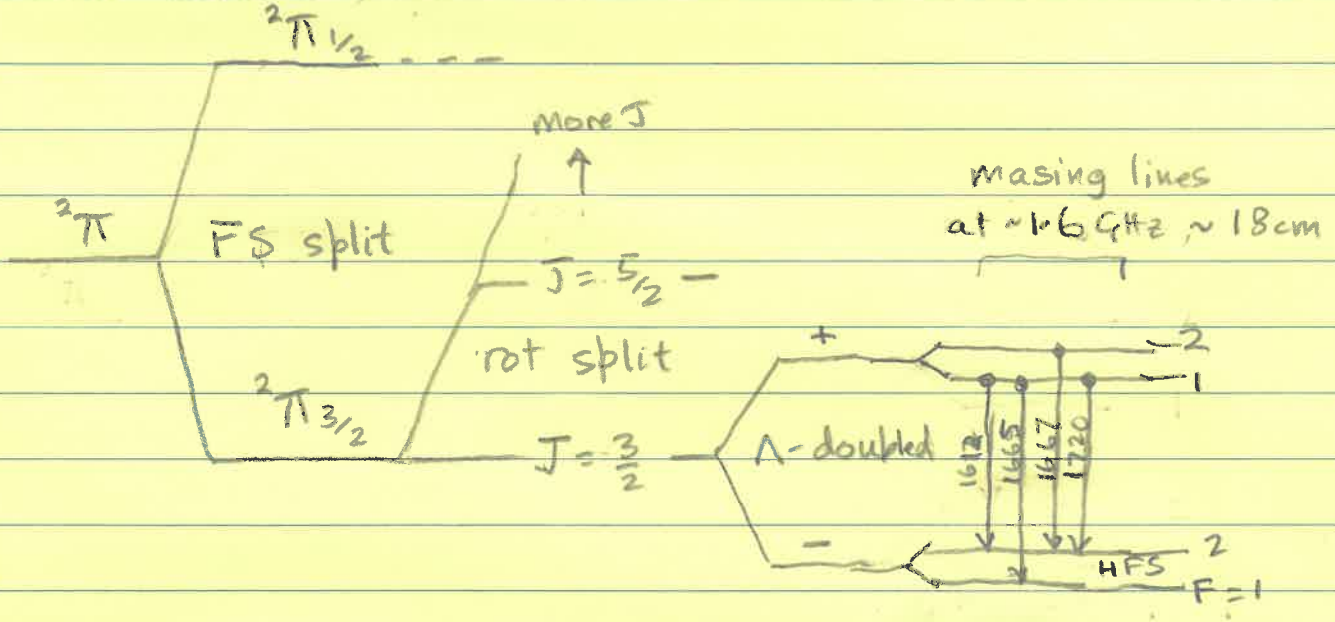

ratios in optically thin limit = 1:5:9:1

thick 1:1:1:1

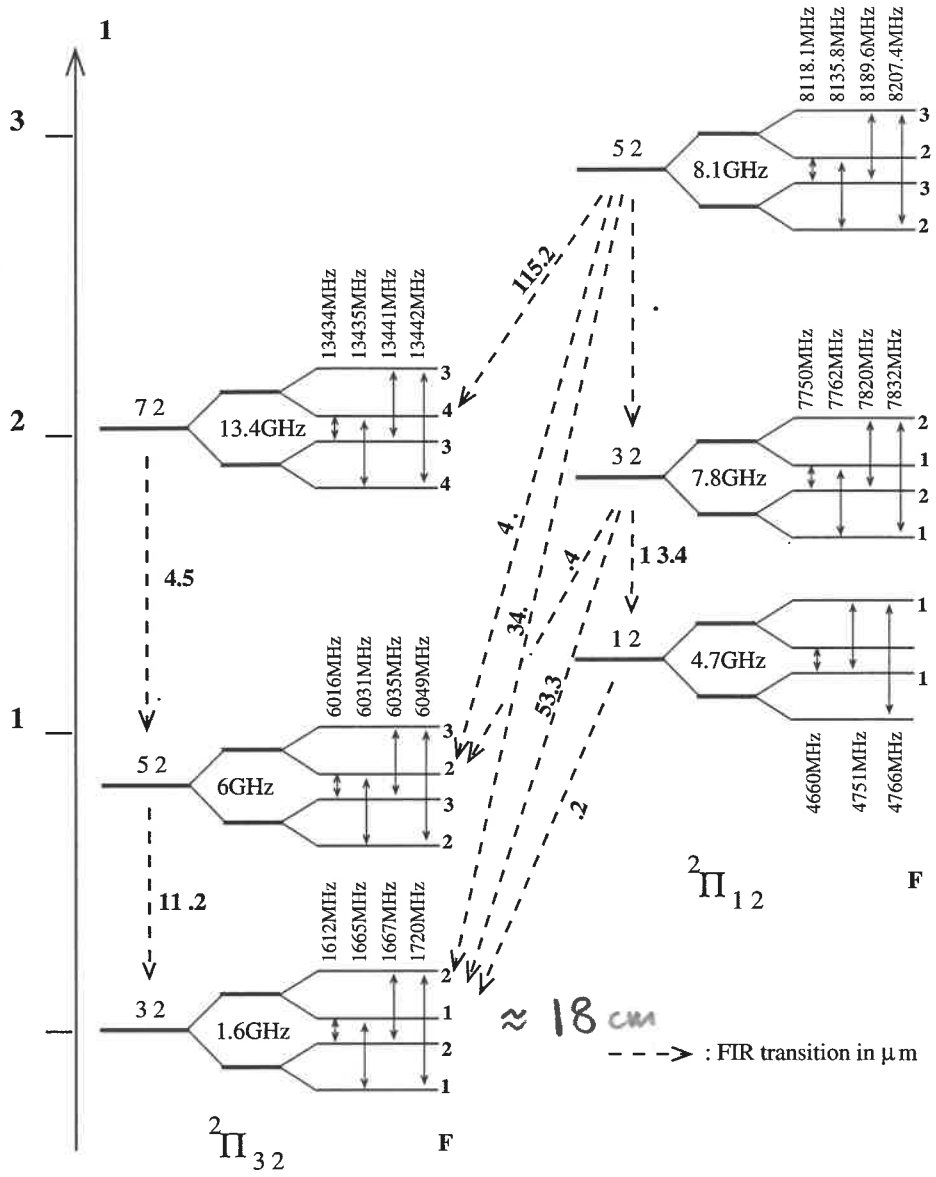

Fig. 1. The energy level diagram for the $^2\Pi_{3/2}$ and $^2\Pi_{1/2}$ ladders of OH. Λ doubling (not to scale) and parities are shown in each case. Transitions between the $F = 3$ and 2 hyperfine levels, for $^2\Pi_{3/2}$, $J = 5/2$, give rise to the four 6 GHz lines.

used a position switching observing mode with the reference position offset by 600″ in longitude from the source position (the half-power beamwidth of the telescope at 6 GHz is 130″). The new auto-correlator AK90 was split into 2 bands of 20 MHz each thus allowing us to simultaneously observe the 2 main lines and the two satellites lines of the $J = 5/2$ state. There were 4096 channels per band giving a channel separation of 4.9 kHz and thus an effective spectral velocity resolution of 0.29 km s^{-1}. Proper functioning of the system was checked by observations of the strong 5 cm OH emission from the two compact HII regions W3(OH) and ON1 (see Table 1).

Calibration of the data followed the procedure used in the 6 GHz survey of star-forming regions made by Baudry et al. (1997). OH spectra were calibrated in terms of the noise source coupled to one polarization channel and the flux density scale was determined by observations of NGC 7027 (Ott et al. 1994). The noise tube was calibrated in Jy assuming that the 6 GHz flux density of NGC 7027 was 5.9 Jy. We estimate that the flux density scale uncertainty is within 10%. All spectra were calibrated in terms of single polarization flux densities. This is one-half of the two polarization flux density. For possible 5 cm radio interference, we proceeded as in Baudry et al. (1997).

Our input catalog is listed in Table 1. It is based on 18 cm OH data. We selected sources which clearly exhibit the 1612 MHz satellite line and/or the 1665/1667 main lines. By these means we obtained targets with noticeable amounts of OH molecules and IR photons, that are not excessively distant in order to be detected.

The sources are essentially OH Miras with thin or moderately thick envelopes, and thick OH/IR objects. Bright Miras with both satellite and main lines were selected, from the Sivagnanam et al. (1988) comprehensive OH survey of the 1-kpc solar neighborhood. Most of them are also known as 22 GHz water maser sources. From the David et al. (1993)

Conditions to obtain maser

(a) At least 3 levels, Why?

(b) Non-TE conditions leading to $n_2/n_1 > g_2/g_1$.

(c) Large column density to amplify maser.

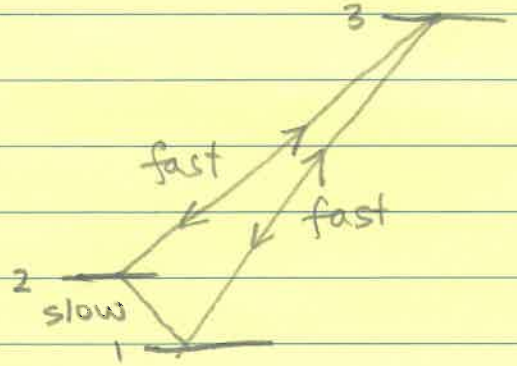

exc temperature

$$\frac{n_2/g_2}{n_1/g_1} = \frac{n_2/g_2}{n_3/g_3} \Big/ \frac{n_1/g_1}{n_3/g_3} = \frac{e^{E_{32}/kT_{32}}}{e^{E_{31}/kT_{31}}}$$

$$= e^{E_{32}/kT_{32} - E_{31}/kT_{31}} = e^{E_{21}/kT_{21}}$$

> 1 masing condition

if $\frac{E_{32}}{T_{32}} > \frac{E_{31}}{T_{31}}$

$$T_{21} = \frac{E_{21}}{E_{32}/T_{32} - E_{31}/T_{31}}$$

ie $\boxed{\frac{T_{31}}{T_{32}} > \frac{E_{31}}{E_{32}}}$

Maser pumping mechanisms

1. Radiative
2. Collisional

1. Radiative pump

Warm dust inside molecular cloud emits in IR with blackbody $B_\nu(T_{dust})$

Molecule inside cloud sees

$$I_\nu \approx B_\nu (1 - e^{-\tau_\nu})$$

$$\rightarrow \begin{cases} B_\nu & \text{large } \tau_\nu, \text{ blue} \\ \tau_\nu B_\nu & \text{small } \tau_\nu, \text{ red} \end{cases}$$

ie red light escapes cloud, blue light scatters inside it.

Result $T_{31} > T_{32}$

This is probably the mechanism that causes OH masers in circumstellar envelopes of Mira variable stars, since maser intensity varies in phase with star.

2. Collisional pump

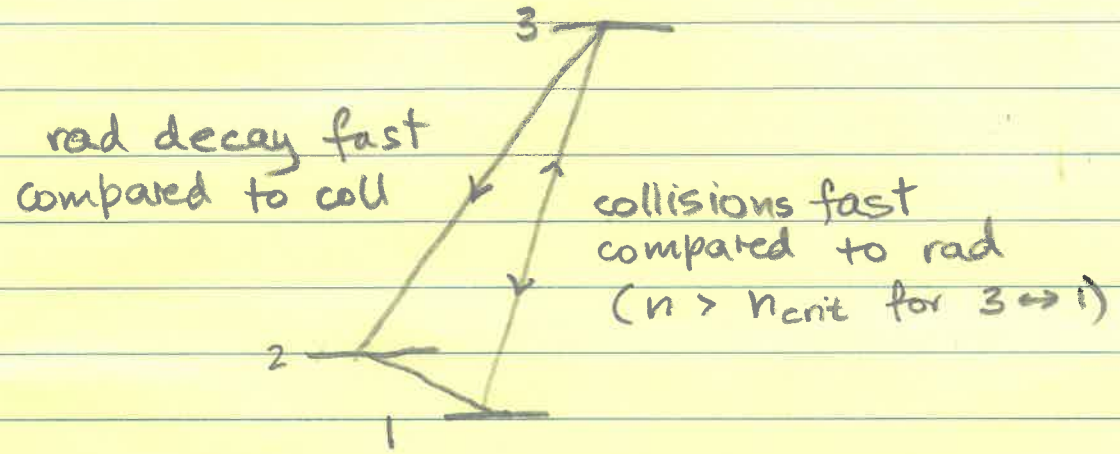

So T_{31} = kinetic temperature of colliders

T_{32} = colder

Result $T_{31} > T_{32}$

Maser radiative transfer

Recall RTE

$$\frac{\partial I_\nu}{\partial \tau_\nu} + I_\nu = S_\nu$$

S_ν ← source func $\frac{j_\nu}{\kappa_\nu}$

In radio, traditionally use T_ν defined by

$$I_\nu \equiv \frac{2\nu^2 kT}{c^2} \qquad \text{Rayleigh-Jeans limit}$$

So $$\frac{\partial T_\nu}{\partial \nu} + T_\nu = T_{ex}$$

Unsaturated case — most astron masers unsat

Maser intensity does not affect level populations (ie n_1 & n_2)

$$S_\nu = \frac{j_\nu}{\kappa_\nu} = \frac{n_2 A_{21}}{n_1 B_{12} - n_2 B_{21}} \qquad \frac{\phi_\nu}{\phi_\nu} \to 1$$

spont em; abs; stim em

$$= \frac{2h\nu_{21}^3}{c^2} \frac{1}{e^{h\nu_{21}/kT_{21}} - 1}$$

So

$$T_{ex} = \frac{S_\nu}{2\nu^2 k/c^2} = \frac{h\nu_{21}}{k} \frac{1}{e^{h\nu_{21}/kT_{21}} - 1} \qquad e^{\cdots} \to 0$$

In usual R-J limit $h\nu_{21} \ll kT_{21}$

this would give $T_{ex} = T_{21}$.

But here T_{21} is -ve and $h\nu_{21} \gg |kT_{21}|$??

so $$T_{ex} \approx -\frac{h\nu_{21}}{k} = -\frac{hc}{k\lambda_{21}} = -.08\ K.$$

For $\lambda_{21} \approx 18$ cm

"molecular" line profile

In j_ν and κ_ν

$n\phi_\nu = \frac{dn}{d\nu}$ = # density of molecules in interval $d\nu$ of frequency.
molecular

The profile ϕ_ν is determined by the velocity distrib of molecules, typically

$$\phi_\nu = \frac{1}{\sqrt{\pi}\,\Delta\nu_D} \exp\left(-\frac{\Delta\nu^2}{\Delta\nu_D^2}\right)$$

$\Delta\nu_D$: Doppler

For constant T_{ex}, solution of RTE is

$$T_\nu = T_{bg} e^{-\tau_\nu} + T_{ex}(1 - e^{-\tau_\nu})$$

background eg CMB, $T_{CMB} \approx 3K$.

For maser, $\tau_\nu < 0$ and $T_{ex} < 0$

In opt. thin regime $|\tau_\nu| \ll 1$

$$T_\nu \approx T_{bg} + (T_{bg} + |T_{ex}|)|\tau_\nu|$$

In opt. thick regime $|\tau_\nu| \gg 1$

$$T_\nu \approx (T_{bg} + |T_{ex}|) e^{|\tau_\nu|}$$

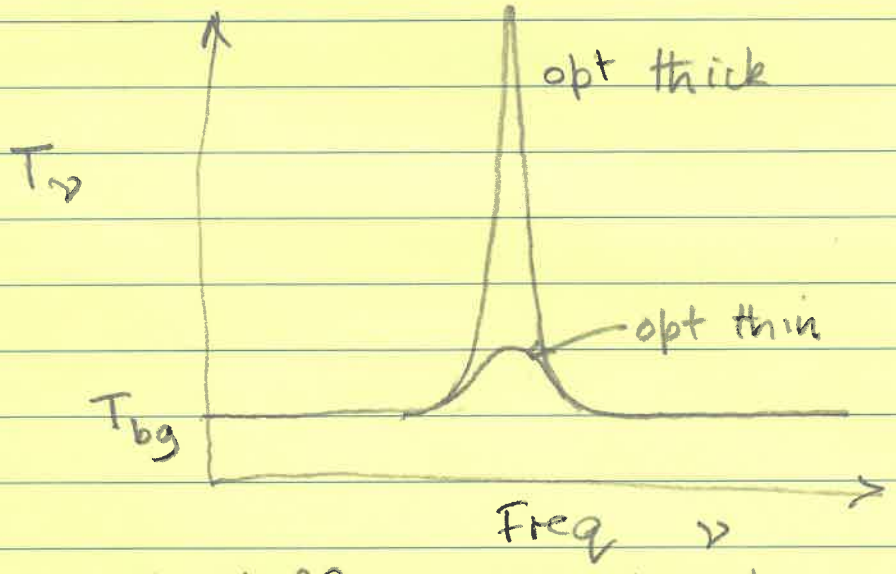

Small differences in atomic line profile ϕ_ν exponentiated out of proportion in obs line profile

$$T_\nu = (T_{bg} + |T_{ex}|) e^{|\tau_0|\phi_\nu}$$

(ϕ_ν: atomic line profile; τ_0: opt depth line ctr)

$\Rightarrow$

1. Non-gaussian obs line profiles with narrow peaked core
2. Strong geometrical effects
   - prefer directions with large $|\tau_\nu|$, with small velocity differences.

Saturated case

Eventually maser intensity I_ν grows strong enough to affect number densities n in various levels.

Do eg. 3-level atom problem.

Typically find

$$T_\nu \propto \tau_\nu \quad \text{instead of} \quad e^{\tau_\nu}$$